01 May 2007

Laser-Assisted Bremsstrahlung for Circular and Linear Polarization

Stephan Schnez

Erik Lotstedt

Ulrich D. Jentschura
Missouri University of Science and Technology, ulj@mst.edu

Christoph H. Keitel

Recommended Citation

S. Schnez et al., "Laser-Assisted Bremsstrahlung for Circular and Linear Polarization," *Physical Review A - Atomic, Molecular, and Optical Physics*, vol. 75, no. 5, pp. 053412-1-053412-12, American Physical Society (APS), May 2007.
The definitive version is available at https://doi.org/10.1103/PhysRevA.75.053412

Laser-assisted bremsstrahlung for circular and linear polarization

Stephan Schnez, Erik Lötstedt, Ulrich D. Jentschura, and Christoph H. Keitel
Max-Planck-Institut für Kernphysik, Saupfercheckweg 1, D-69117 Heidelberg, Germany
(Received 8 January 2007; published 18 May 2007)

We numerically evaluate the cross sections for spontaneous bremsstrahlung emission in a laser field for both circular and linear laser polarization, in a regime where the classical ponderomotive energies for the considered laser intensities are considerably larger than the rest mass of the electron. A fully relativistic quantum-electrodynamic approach using the Volkov solutions of an electron in an external field and Dirac-Volkov propagators for the intermediate electrons is applied. We compare circular to linear polarization and point out several interesting features of the laser-dressed cross sections. Regularizations in both electron and photon propagators are required. Specifically, imaginary mass and energy shifts of the electron must be implemented near resonances which correspond to Doppler-shifted harmonics of the laser frequency. We also introduce a screening to the Coulomb potential in order to avoid long-range Coulomb infinities at zero momentum transfer.

DOI: 10.1103/PhysRevA.75.053412 PACS number(s): 34.80.Qb, 41.60.Cr, 42.55.−f

I. INTRODUCTION

Laser-assisted processes in atomic physics have drawn considerable attention since the emergence of the first lasers in the 1960s. This interest is due to the newly discovered and exciting features of laser-matter interaction such as above-threshold ionization [1,2] and higher harmonic generation [3,4]. A detailed description of the historic steps of theory and experiments leading to the status quo can be found in the review paper [5]. In view of today's high-intensity lasers, the classical ponderomotive energy of an electron or an equivalent particle in the laser field can be of the order of or even much larger than its rest mass. Thus, it is inevitable to employ a fully relativistic, quantum-electrodynamic approach to describe laser-matter interactions adequately in the strong field domain.

The first laser-assisted processes which were studied using quantum electrodynamics (QED) were first-order processes: laser-induced Compton scattering [6–8] and laser-assisted Mott scattering [9,10]. The next obvious step was to consider second-order processes. The first process of this kind to be considered in the literature was laser-assisted electron-electron scattering (Møller scattering, see Refs. [11–13]). We should also mention that higher-order QED effects in static magnetic and electric fields have been intensely studied, see e.g., [14–16]. Recently there has also been proposals that laser-driven particles can show signatures of the Unruh effect [17–19].

In this paper, we treat another second-order process in an external laser field, namely laser-assisted bremsstrahlung. In [20], a first discussion of this process in the limit of a nonrelativistic electron was given. Another interesting case which is related to laser-assisted bremsstrahlung is an electron which is bound in a Coulomb field and exposed to a circularly polarized electromagnetic field. This also leads to spontaneous emission of radiation [21,22]. A formalism for the extension of the calculation of laser-assisted bremsstrahlung to the relativistic regime using QED was given in [23] for the first time and again in [24,25]; however, no actual evaluation of the resulting cross section was carried out. In a preceding paper [26], a numerical approach for the evaluation of the bremsstrahlung cross section in a linearly polarized field was developed. Here, we take a further step ahead and compare the cross sections for linear and circular polarization. In principle, we would expect not only quantitative but also qualitative differences in the cross section, because for linear polarization the classical electron trajectory is described by a zigzag-like trajectory, whereas the classical trajectory is similar to a helix in the circular case [27]. Bremsstrahlung is described by the two Feynman diagrams in Fig. 1.

In the first one, the initial electron first interacts with the Coulomb field and then emits the bremsstrahlung photon. The situation is reversed in the second diagram. Since there is no possibility to experimentally distinguish which of the two processes takes place, both amplitudes must be added up coherently. The laser-dressed electron is taken into account in the usual way, i.e., by using the Volkov solutions [28,29] of the Dirac equation in an external plane wave field.

The calculation of second-order processes implies the treatment of a propagator. For bremsstrahlung, we encounter an electron propagator (see Fig. 1), in contrast to a photon propagator as in Møller scattering. Since the virtual photons cannot interact with the laser photons unless virtual excitations of the electron-positron field are considered, the free photon propagator is a good approximation. However, in the bremsstrahlung case, the intermediate electron interacts strongly with the photons of the intense laser field. The free electron propagator is not a suitable choice as it is intuitively clear and demonstrated numerically in [26]. We implement

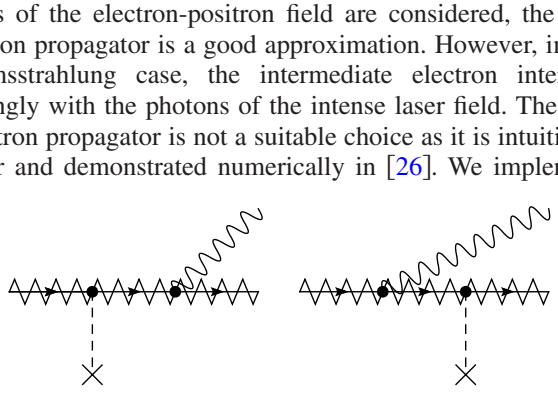

FIG. 1. The two Feynman diagrams describing laser-assisted bremsstrahlung emission in a Coulomb field. The external laser field is denoted by the nonstandard notation of a zigzag line, the virtual Coulomb photon is drawn as a dashed line. Time evolves from left to right.

the full, laser-dressed electron propagator in our formalism by using certain expressions derived in [30–32].

It should be mentioned that the cross section we derive is a generalization of the well-known bremsstrahlung cross section first derived by Bethe and Heitler in Ref. [33]. We expect our results to agree with the Bethe-Heitler cross section in the limit of a vanishing laser field, while even qualitative differences are expected as the laser is "turned on."

From laser physics with bound electrons we know that recollision effects are essential to explain above-threshold ionization and higher-harmonic generation. According to the three-step model [34], an atom is ionized by a laser in a first step. In the second step, the free electron is accelerated classically in the laser field and recollides with the nucleus in the third and final step. This recollision generates the radiation. The question arises whether we must consider recollision effects in laser-assisted bremsstrahlung as well. As we show in Appendix B below, this is not the case for an electron with a ponderomotive energy of the order of its rest mass because the radiation pressure inhibits any conceivable recollision of the electron with the nucleus.

In this paper, we use the same conventions and notations as in [26]. In particular, we apply natural units with $\hbar=c=\epsilon_0=1$. The fine-structure constant is $\alpha=e^2/(4\pi)$. The four-vector product is denoted by a dot: $a\cdot b=g_{\mu\nu}a^\mu b^\nu=a^0b^0-\boldsymbol{a}\cdot\boldsymbol{b}$ with the metric tensor $g=\mathrm{diag}(1,-1,-1,-1)$. For the Feynman dagger, we use the following notation: $\hat{F}=F\cdot\gamma$. The more conventional notation of a slash for denoting the Feynman dagger as in $\not{p}$ is not suitable for some capital letters employed here. For example, $\not{A}$ is hard to read and could lead to some confusion. The Dirac adjoint is denoted by the standard notation $\bar{u}=u^\dagger\gamma^0$ for a bispinor u and $\bar{\Lambda}=\gamma^0\Lambda^\dagger\gamma^0$ for a (4×4)-matrix Λ. The electron mass and charge are given by m and $e=-|e|$, respectively.

The outline of this paper is the following. First, we will extensively discuss the cross section for circular polarization in Sec. II A. Then, we will shortly point out the main differences of linear polarization compared to the circular case in Sec. II B. After this theoretical part, we will present results of our numerical evaluations: the imaginary mass shift is treated in Sec. III A, different spectra are shown in Sec. III B, and some rather curious phenomena occurring in the differential cross section are discussed in Sec. III C. Concluding remarks are reserved for Sec. IV.

II. THEORETICAL DERIVATION OF THE BREMSSTRAHLUNG CROSS SECTION

A. Circular polarization

The four-vector potential for both linearly and circularly polarized plane wave fields can be given in a unified notation as

$$A^\mu(\phi)=a(\epsilon_1^\mu\cos\phi+\delta\epsilon_2^\mu\sin\phi), \tag{1}$$

with linear polarization for $\delta=0$ and circular polarization for $\delta=1$. Plane waves only depend on space and time via the four-vector product of the wave vector k of the laser field and the position vector x:

$$\phi=k\cdot x. \tag{2}$$

We work in the radiation gauge so that we have two real laser polarization vector $\boldsymbol{\epsilon}_1$ and $\boldsymbol{\epsilon}_2$ with $\epsilon_i^0=0$, $\boldsymbol{k}\cdot\boldsymbol{\epsilon}_i=0$, and $\boldsymbol{\epsilon}_i\cdot\boldsymbol{\epsilon}_j=-\delta_{ij}$ $(i,j=1,2)$. In this section, we only consider circular polarization. Then, we especially find that A^2 is a constant, $A^2=-a^2$. The initial and final electron states in the laser field are described by wave functions $\psi_{i,f}$ which fulfill the Dirac equation with an external potential coupled to it:

$$[i\hat{\partial}-e\hat{A}(\phi)-m]\psi_{i,f}(x)=0. \tag{3}$$

The well-known Volkov wave functions are solutions to this equation [29]; they read [35]:

$$\psi_{p,r}(x)=\sqrt{\frac{m}{QV}}\left(1+\frac{e\hat{k}\hat{A}(\phi)}{2(k\cdot p)}\right)u_r(p)e^{iS_p[\phi]} \tag{4}$$

with

$$S_p[\phi]=-p\cdot x-\int_0^\phi\left(e\frac{p\cdot A(\phi')}{k\cdot p}-e^2\frac{A^2(\phi')}{2(k\cdot p)}\right)d\phi'. \tag{5}$$

In the free Dirac bispinor $u_r(p)$, which enters into the Volkov solutions, p is the asymptotic momentum of the particle outside the laser field, which is generalized naturally to an *effective momentum*

$$q=p+\frac{e^2a^2}{2k\cdot p}k \tag{6}$$

within the laser field. The zero component $Q\equiv q^0$, i.e., the effective energy, already appears in the normalization factor of the Volkov wave function. We employ a box normalization with a normalization volume V. The effective momentum leads to an effective mass $m_*^2=q^2=m^2+e^2a^2$. We end up with a modified relativistic energy-momentum relation, $Q^2=|\boldsymbol{q}|^2+m_*^2$, which is obtained by expressing the laser-free relation $p^2=m^2$ in terms of Q.

We expand the Volkov solutions in so-called generalized Bessel functions:

$$\begin{aligned}\psi_{p,r}(x)&=\sqrt{\frac{m}{QV}}\sum_{s=-\infty}^{\infty}\exp[-i(q-sk)\cdot x]\left(B_s^0(\xi,\eta)\right.\\&\left.+\frac{ea\hat{k}}{2k\cdot p}[\hat{\epsilon}_1B_s^1(\xi,\eta)+\hat{\epsilon}_2B_s^2(\xi,\eta)]\right)u_r(p)\\&\equiv\sqrt{\frac{m}{QV}}E_p(x)u_r(p).\end{aligned} \tag{7}$$

The last line implicitly defines the (4×4)-matrix $E_p(x)$. The generalized Bessel functions are given by sums over products of Bessel functions of the first kind,

$$B_s^0(\xi,\eta)=\sum_{n=-\infty}^{+\infty}i^nJ_{s-n}(\xi)J_n(\eta),$$

$$B_s^1(\xi,\eta)=\frac{1}{2}[B_{s-1}^0(\xi,\eta)+B_{s+1}^0(\xi,\eta)],$$

$$B_s^2(\xi,\eta) = \frac{1}{2i}[B_{s-1}^0(\xi,\eta) - B_{s+1}^0(\xi,\eta)]. \tag{8}$$

In the circular case, a simplification of the generalized Bessel function is possible, which leads to a full reduction to ordinary Bessel functions. This is explained in Appendix A in addition to other properties of Bessel functions. A corresponding simplification for linear polarization is not possible, as pointed out below. The arguments of the generalized Bessel functions connect the effective four momentum of the electron with the laser polarization vectors and are defined by

$$\xi_q = -ea\frac{q\cdot\epsilon_1}{k\cdot q} \quad \text{and} \quad \eta_q = ea\frac{q\cdot\epsilon_2}{k\cdot q}. \tag{9}$$

We now must consider the electron propagator $G(x_2,x_1)$ in a laser field. Electron propagators are Green's functions to the Dirac equation, and $G(x_2,x_1)$ solves the differential equation

$$(i\hat{\partial} - e\hat{A} - m)G(x_2,x_1) = \delta(x_2 - x_1). \tag{10}$$

There are several approaches to find a solution to the above equation; one approach is discussed in [36]. According to [30,31], we have

$$G(x_2,x_1) = \int \frac{d^4p}{(2\pi)^4} E_p(x_2)\frac{\hat{p}+m}{p^2-m^2+i\epsilon}\bar{E}_p(x_1), \tag{11}$$

with the definition of E_p according to Eq. (7).

In the limit $a\to 0$, we expect to retrieve the free solutions. The effective four momentum (6) takes the same value as the free momentum, $q^\mu = p^\mu$. Obviously, the arguments of the generalized Bessel functions (9) are equal to zero in this case. Hence, we get $B_s^0(0,0) = \delta_{s0}$ as it is derived in Appendix A. The Volkov solution goes over to $\psi_{p,r}(x) = \sqrt{m/(EV)}u_r(p)\exp(-ipx)$, the solution of the free Dirac equation. We see that in this limit $E_p(x) = \exp(-ipx)$, the laser-dressed electron propagator can thus most easily be written as

$$G(x_2,x_1) \xrightarrow{a\to 0} \int \frac{d^4p}{(2\pi)^4}\frac{1}{\hat{p}-m+i\epsilon}e^{-ip(x_2-x_1)}, \tag{12}$$

which clearly is the free electron propagator. At this stage, we can already conclude that our ansatz will go over to the free—i.e., Bethe-Heitler—cross section in the limit of a vanishing laser field. Numerical tests of our program fully confirm these formal considerations.

In order to incorporate screening, we employ a Yukawa potential instead of the more conventional Coulomb potential,

$$A_Y^\mu(x) = (2\pi)^{-4}\int d^4q A_Y^\mu(q)\exp(-iqx), \tag{13}$$

where the Fourier-transformed Yukawa potential

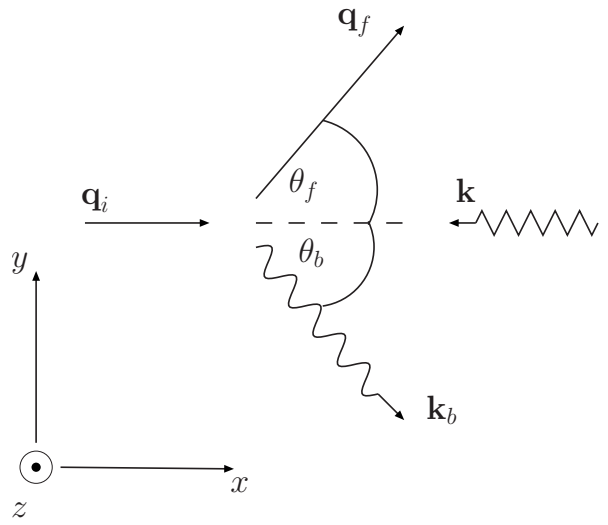

FIG. 2. The scattering geometry: The initial electron with four momentum q_i and the laser photons with k are counterpropagating and (anti)parallel to the x axis. The final electron with q_f and the bremsstrahlung photon with k_b are projected onto the xy plane in this figure; thus, only the polar angles θ_f and θ_b are displayed. The azimuthal angles are called ρ_f and ρ_b, respectively.

$$A_Y^\mu(q) = 2\pi\delta(q^0)\left(\frac{-Ze}{\boldsymbol{q}^2+\ell^{-2}}\right)\delta^{\mu 0} \tag{14}$$

is used to describe the interaction of the electron with the nucleus of charge $-Ze$, where $-e=|e|$ is the charge of a single proton. The concrete value of the screening length ℓ depends on the experimental setup. For $\ell\to\infty$, we of course retrieve the Coulomb potential [37]. The reason why we employ a screened Yukawa potential is explained below. The four-vector potential of the emitted bremsstrahlung photon with wave vector $k_b=(\omega_b,\boldsymbol{k}_b)$ is written as $A_{b,\lambda}^\mu(x) = \varepsilon_{b,\lambda}^\mu \exp(ik_b\cdot x)/(\sqrt{2\omega_b V})$, again in a box normalization. The integer λ can adopt the values 1 and 2 and thus distinguishes between the two possible polarization directions of the bremsstrahlung photon.

We can now write down the transition amplitudes for laser-assisted bremsstrahlung applying Feynman rules for coordinate space to the diagrams in Fig. 1,

$$S_{fi} = e^2\int d^4x_1\int d^4x_2\bar{\psi}_f(x_2)\{[-i\hat{A}_{b,\lambda}(x_2)]iG(x_2,x_1) \times[-i\hat{A}_Y(x_1)] + [-i\hat{A}_Y(x_2)]iG(x_2,x_1)[-i\hat{A}_{b,\lambda}(x_1)]\}\psi_i(x_1). \tag{15}$$

We consider a scattering geometry which is of special interest for experiments, namely the head-on collision of incoming electrons and laser photons (Fig. 2). The four-momenta are given as follows. For the initial electron, we have $q_i=(Q_i,|\boldsymbol{q}_i|,0,0)$, whereas for the final electron state, we use $q_f=(Q_f,|\boldsymbol{q}_f|\cos\theta_f,|\boldsymbol{q}_f|\sin\theta_f\cos\rho_f,|\boldsymbol{q}_f|\sin\theta_f\sin\rho_f)$, and the laser photon has $k=(\omega,-\omega,0,0)$, whereas the bremsstrahlung photon is characterized by $k_b=(\omega_b,\omega_b\cos\theta_b,\omega_b\sin\theta_b\cos\rho_b,\omega_b\sin\theta_b\sin\rho_b)$. Of

course, $|\boldsymbol{q}_{i,f}|=\sqrt{Q_{i,f}^2-m_*^2}$. The polarization vectors must be orthogonal to the wave vector and to each other with zero time component in the radiation gauge. Thus, we have $\varepsilon_{b,1}=(0,0,-\sin\rho_b,\cos\rho_b)$ and $\varepsilon_{b,2}=(0,-\sin\theta_b,\cos\theta_b\cos\rho_b,\cos\theta_b\sin\rho_b)$. The simplest choice for $\boldsymbol{\epsilon}_1$ and $\boldsymbol{\epsilon}_2$ would be (0, 0, 1, 0) and (0, 0, 0, 1). However, an equivalent and in fact more convenient choice turns out to be given by $\boldsymbol{\epsilon}_1=(0,0,\cos\rho_f,\sin\rho_f)$ and $\boldsymbol{\epsilon}_2=(0,0,-\sin\rho_f,\cos\rho_f)$. Since the incoming electron and the laser photons are counterpropagating, $\boldsymbol{q}_i$ is perpendicular to the laser polarization vectors $\boldsymbol{\epsilon}_1$ and $\boldsymbol{\epsilon}_2$. Hence, we obtain $\eta_{q_i}=\xi_{q_i}=0$ anyway. Moreover, because of the more sophisticated choice of $\boldsymbol{\epsilon}_1$ and $\boldsymbol{\epsilon}_2$, we have $\eta_{q_f}=0$ because it is proportional to $q_f\cdot\epsilon_2=-(q_f)_y\cdot(\epsilon_2)_y-(q_f)_z\cdot(\epsilon_2)_z=0$. Consequently, the (generalized) Bessel functions in the Volkov states simplify considerably as shown in Appendix A.

The expression for S_{fi} reads as follows:

$$S_{fi}=\frac{2\pi iZe^3m}{\sqrt{2\omega_bQ_iQ_fV^3}}\sum_{n,s=-\infty}^{\infty}\frac{\delta(q_n^0)}{|\boldsymbol{q}_n|^2+\ell^{-2}}\bar{u}_{r_f}(p_f)\times\left(M_{-n-s}^{f,\tilde{p}_f}(\hat{\varepsilon}_{b,\lambda},\xi_{\tilde{p}_f}-\xi_{q_f},\eta_{\tilde{p}_f})\frac{\hat{\tilde{p}}_f-\frac{e^2a^2}{2k\cdot\tilde{p}_f}\hat{k}+m}{\tilde{p}_f^2-m_*^2}\times\bar{M}_{-s}^{i,\tilde{p}_f}(\gamma^0,\xi_{\tilde{p}_f},\eta_{\tilde{p}_f})+M_{-n-s}^{f,\tilde{p}_i}(\gamma^0,\xi_{\tilde{p}_i}-\xi_{q_f},\eta_{\tilde{p}_i})\times\frac{\hat{\tilde{p}}_i-\frac{e^2a^2}{2k\cdot\tilde{p}_i}\hat{k}+m}{\tilde{p}_i^2-m_*^2}\bar{M}_{-s}^{i,\tilde{p}_i}(\hat{\varepsilon}_{b,\lambda},\xi_{\tilde{p}_i},\eta_{\tilde{p}_i})\right)u_{r_i}(p_i)\quad(16)$$

with the four-momentum transfer onto the nucleus $q_n=q_f-q_i-nk+k_b$. The intermediate electron momenta are defined by

$$\tilde{p}_f=q_f-(n+s)k+k_b,\quad(17)$$

$$\tilde{p}_i=q_i-sk-k_b.\quad(18)$$

The (4×4)-matrix M describes the interaction with the nucleus and the emission of the bremsstrahlung photon, respectively,

$$M_t^{j,q}(X,\xi,\eta)=\left(X+\frac{e^2a^2}{4(k\cdot p_j)(k\cdot q)}\hat{k}X\hat{k}\right)B_t^0(\xi,\eta)+\left(\frac{ea}{2k\cdot q}X\hat{k}\hat{\epsilon}_1+\frac{ea}{2k\cdot p_j}\hat{\epsilon}_1\hat{k}X\right)B_t^1(\xi,\eta)+\left(\frac{ea}{2k\cdot q}X\hat{k}\hat{\epsilon}_2+\frac{ea}{2k\cdot p_j}\hat{\epsilon}_2\hat{k}X\right)B_t^2(\xi,\eta).\quad(19)$$

Here, M is a (4×4) matrix with three indices and three arguments. The first index j can take the values i and f in order to differ between the initial and final electron. The second upper index q is equal to either $\tilde{p}_i$ or $\tilde{p}_f$ according to the corresponding propagator, whereas t is a summation index for the Bessel functions. The first argument of M, which is X, constitutes a (4×4)-matrix and takes the values $\hat{\epsilon}_{b,\lambda}$ or γ^0. In the first case, it describes photon emission, in the second case, M is the interaction matrix with the Yukawa potential. The other two arguments ξ and η are given by the coupling of the electron to the laser field, as detailed in the parameters defined in Eq. (9).

The differential cross section is calculated with the well-known formula

$$d\sigma=\frac{V}{|\boldsymbol{v}_i|T}|S_{fi}|^2\frac{Vd^3k_b}{(2\pi)^3}\frac{Vd^3q_f}{(2\pi)^3}\quad(20)$$

with $\boldsymbol{v}_i$ being the initial electron velocity.

We consider an unpolarized electron beam. Then, we must sum over initial and final spins r_i and r_f. The averaging over the initial spin r_i yields a factor $\frac{1}{2}$. Summing over final photon polarization as well finally yields the unpolarized differential cross section $d\bar{\sigma}=\frac{1}{2}\Sigma_{r_i,r_f,\lambda}d\sigma$. If we plug S_{fi} into the expression for the differential cross section, we can rewrite it as a trace. For any (4×4)-matrix Λ, a summation over the magnetic spin projections leads to

$$\sum_{r_i,r_f=1,2}|\bar{u}_{r_f}(p_f)\Lambda u_{r_i}(p_i)|^2=\mathrm{Tr}\left(\Lambda\frac{\hat{p}_i+m}{2m}\bar{\Lambda}\frac{\hat{p}_f+m}{2m}\right).\quad(21)$$

The following relations turn out to be useful: $Q_i|\boldsymbol{v}_i|=|\boldsymbol{q}_i|$, $d^3k_b=\omega_b^2d\omega_bd\Omega_b$, $d^3q_f=|\boldsymbol{q}_f|^2d|\boldsymbol{q}_f|d\Omega_f$, and $Q_fdQ_f=|\boldsymbol{q}_f|d|\boldsymbol{q}_f|$. Two more aspects need to be mentioned. Taking the square of the S-matrix implies multiplying two δ functions with each other, $\delta(q_n^0)\delta(q_{n'}^0)$. Thus, only terms with $n=n'$ contribute. With the help of the well-known substitution $[\delta(q_n^0)]^2\to\frac{T}{2\pi}\delta(q_n^0)$ (see Ref. [29]), we are able to cancel the factors of T. We still must integrate over the energy Q_f of the final electron. Together with the remaining δ function, this yields the energy conservation $Q_f=Q_i+n\omega-\omega_b$. It is straightforward now to write down the differential cross section:

$$\frac{d\bar{\sigma}}{d\Omega_fd\Omega_bd\omega_b}=\frac{\alpha(Z\alpha)^2\omega_b}{8\pi^2}\frac{1}{|\boldsymbol{q}_i|}\sum_{\lambda=1,2}\sum_n\frac{|\boldsymbol{q}_f|}{(|\boldsymbol{q}_n|^2+\ell^{-2})^2}\times\mathrm{Tr}\left[\left(\sum_sP_{n,s}^\lambda\right)(\hat{p}_i+m)\left(\sum_{s'}\bar{P}_{n,s'}^\lambda\right)\times(\hat{p}_f+m)\right]\Theta(Q_f-m_*).\quad(22)$$

The step function ensures that the energy of the outgoing electron is always greater than its rest mass. This is in close analogy to the Bethe-Heitler formula. $P_{n,s}^\lambda$ is equal to the expression in the large parentheses in Eq. (16), and we suppress the dependence of $P_{n,s}^\lambda$ on all of its arguments except for the summation indices n, s, and λ.

The above cross section is differential in the directions of both the final electron and the emitted bremsstrahlung photon and in the energy ω_b of the bremsstrahlung photon. For any experimental test, the electron and the photon would have to be detected in coincidence, and this provides for a considerable challenge. Moreover, we are mainly interested in the bremsstrahlung photon; the electron is just used to "create" it. So, we integrate the differential cross section

over $d\Omega_f$ to get a cross section which is only differential in the direction of the emitted bremsstrahlung photon and in its energy:

$$\frac{d\bar{\sigma}}{d\Omega_b d\omega_b} = \int d\Omega_f \frac{d\bar{\sigma}}{d\Omega_f d\Omega_b d\omega_b}. \tag{23}$$

Of course, this integration can only be done numerically; we employ a Gaussian integration routine. In the following, we use the term *total* cross section for the quantity given on the left-hand side of Eq. (23), which is differential only in the variables of the emitted bremsstrahlung photon (angles and energy). If we use the term *differential* cross section, we refer to the quantity given on the left-hand side of Eq. (22), which is differential in the variables of the final electron state and of the emitted bremsstrahlung photon.

At this point, we insert a little detour and focus on the evaluation of the trace. Using well-known properties of γ-matrices, traces like the one in Eq. (22) can be rewritten as normal four-vector products. However, tracing out an expression like $\mathrm{Tr}[\hat{a}_1\hat{a}_2\cdots\hat{a}_n]$ *a priori* yields $(n-1)!!$ terms [38]. On the other hand, doing the matrix multiplication within the trace explicitly just give $64(n-1)$ terms (each matrix has 16 entries, hence one matrix multiplication gives 16 times 4 terms). Although it is counterintuitive at first glance, it turns out that we end up with less terms to calculate doing explicit matrix multiplication when the number of matrices in the trace is greater than or equal to 10. In our case, we have 16 matrices to multiply which corresponds to more than 2 million terms if we trace them out. Doing the matrix multiplication, we end up with just 576 terms. That is the reason why we choose a plain numerical implementation of the γ-matrices (in the Dirac representation) and calculate all traces by explicit matrix multiplication.

Resonances in the cross section occur whenever the intermediate electron is on-shell, i.e., $\tilde{p}_f^2 = m_*^2$ or $\tilde{p}_i^2 = m_*^2$. We define $\tilde{n}$ and $\tilde{n}_b$ by $k = \omega\tilde{n}$ and $k_b = \omega_b\tilde{n}_b$. Then, the on-shell condition yields

$$\frac{\omega_b}{\omega} = (n+s)\frac{q_f\cdot\tilde{n}}{q_f\cdot\tilde{n}_b - (n+s)k\cdot\tilde{n}_b} \tag{24}$$

for $\tilde{p}_f$ and the first propagator and

$$\frac{\omega_b}{\omega} = s\frac{q_i\cdot\tilde{n}}{sk\cdot\tilde{n}_b - q_i\cdot\tilde{n}_b} \tag{25}$$

for $\tilde{p}_i$. If we especially choose $\tilde{n}_b = \tilde{n}$, the two equations simplify to $\omega_b/\omega = n+s$ and $\omega_b/\omega = -s$. Hence, the resonances occur at integer multiples of the laser frequency or, in other words, we obtain harmonic radiation [39]. The physical nature of the resonances can be explained as follows. When the frequency of the emitted photon satisfies the on-shell relation (24) or (25), the second order process described by the diagrams in Fig. 1 splits into two successive first-order processes: laser-induced Compton scattering and laser-assisted Coulomb scattering, and thus perturbation theory breaks down. In the presence of the laser field, the electron can emit radiation even without interacting with the Coulomb field. Without regularization, the cross section is infinite at a resonance. This singular behavior results from integration over an infinitely large space-time volume in Eq. (15).

We implement an imaginary mass shift to get finite resonance peaks [23,30], $m \to m - i\Gamma_m/2$ with

$$\Gamma_m(k\cdot\tilde{p}) = \frac{\tilde{p}^0}{m} W_\gamma(k\cdot\tilde{p}), \tag{26}$$

where $\tilde{p}^0$ is the zero component of the four momentum $\tilde{p}$ of the intermediate electron in the denominator of the propagators in Eq. (16). W_γ with argument $(k\cdot\tilde{p})$ is the total probability of photon emission by an electron with four-momentum $\tilde{p}$ in a laser field with laser photons possessing four momentum k. It is crucial to also introduce an imaginary energy shift $\Gamma_{\tilde{E}}/2$ so that a modified on-shell condition can be restored,

$$(\tilde{E} - i\Gamma_{\tilde{E}}/2)^2 = (m - i\Gamma_m/2)^2 + \boldsymbol{q}^2. \tag{27}$$

To first order, we find $\Gamma_{\tilde{E}} = \frac{m}{\tilde{E}}\Gamma_m$. We define the shifted effective four momentum $q^\Gamma = [Q - i(m/Q)\Gamma_m(k\cdot q)/2, \mathbf{q}]$.

W_γ is derived in [29] for circular polarization and can be approximated by a linear function of $(k\cdot\tilde{p})$ to a very high accuracy in our range of interest. This will become clear from the later discussion. Thus, it turns out that $\Gamma_m = b_a(k\cdot\tilde{p})$. The slope b_a depends on the laser intensity a. In the limit of small a, our results agree with [32,40].

The shifted electron propagator then reads (to first order in Γ_m)

$$\begin{aligned}\tilde{p}_f^2 - m_*^2 \to [q_f^\Gamma - (n+s)k + k_b]^2 - m_*^2 + im\Gamma_m(k\cdot\tilde{p}_f)\\ = -2(n+s)q_f\cdot k + 2q_f\cdot k_b - 2(n+s)k\cdot k_b\\ + i\frac{m}{Q_f}\Gamma_m(k\cdot q_f)((n+s)\omega - \omega_b) + im\Gamma_m(k\cdot k_b),\end{aligned} \tag{28}$$

because $k\cdot\tilde{p}_f = k\cdot q_f + k\cdot k_b$ and Γ_m is assumed linear in its argument. For the second propagator, one easily obtains the corresponding result [for $f \to i$ in the first line of Eq. (28)].

Some remarks are in order regarding the inclusion of the finite widths of the intermediate states in the Dirac-Volkov propagator, as suggested in [12,23,32] and explicitly used for the numerical evaluation performed in [26]. First, we recall that our calculation is valid only if the electron spends enough time in the region where the laser field is present. For our approach to be correct, this time period should be much larger than the period of the laser field and the spatial extent of the laser focus region should be much larger than the laser wavelength. In this case, it is permissible to use the employed approximation of a laser pulse of infinite duration (continuous-wave) and of infinite spatial extension. In the regime of short laser pulses, our approximation breaks down, and another approach is called for. A pulsed laser field can in principle be dealt with by the same theoretical framework as is used in this paper, since Volkov wave functions exist also for laser vector potentials of the form

$$A^\mu(\phi) = ag(\phi)(\epsilon_1^\mu\cos\phi + \delta\epsilon_2^\mu\sin\phi), \tag{29}$$

where $g(\phi)$ is an envelope function. Laser-induced Compton scattering in a pulsed laser field for the case when $g(\phi)$ is a

slowly varying function was treated in [41]. For the radiative corrections, implemented by including Γ_m in the propagator denominator, to be the dominant regularization mechanism, it is crucial that the electron is allowed to travel in the laser field for a time span τ longer than $1/\Gamma_m$ before (or after) scattering at the Coulomb field. If this is not the case, the electron will not have enough time to radiate independently of the Coulomb interaction, and the peaks will necessarily disappear. As will follow from Fig. 3, in the regime of parameters we are considering we have $\Gamma_m \sim \omega$. The electron travels in the laser field over many wavelengths by assumption, and thus $\tau \gg 1/\Gamma_m$ as required. We also note that in an actual experiment, other external parameters, such as frequency width of the laser $\Delta\omega$ and width of the energy distribution of the incoming electron ΔE, may additionally provide for a cutoff for the resonances. For the radiative corrections to dominate as damping mechanism here, it is required that ΔE and $\Delta\omega$ are smaller than Γ_m. In our example later, where $\Gamma_m \sim \omega$, $\omega = 1.17$ eV and $E = 5.11$ MeV, this condition may be difficult to realize for ΔE.

Returning to the discussion of the resonance conditions, it turns out that one can find a specific scattering angle θ_f of the final electron so that the momentum transfer q_n onto the nucleus is zero. This leads to momentum conservation $q_f = q_i + nk - k_b$ which is equivalent to $q_i \cdot k_b = n q_f \cdot k$. This, in turn, is equal to the on-shell constraints (24) and (25) if we express it only in terms of q_i or q_f. Formally, it results in

$$\frac{d\bar{\sigma}}{d\Omega_b d\omega_b} \to \infty \tag{30}$$

for $|\boldsymbol{q}_n| = 0$. Hence, if we employed a Coulomb potential, we would get a singularity *at every resonance* in the total cross section (integration over $d\Omega_f$). The screened Coulomb or Yukawa potential avoids this by implementing the screening length ℓ. The Yukawa potential is a modified Coulomb potential for small momentum transfer. The screening length ℓ, however, enters the theoretical formalism as an external parameter which must be deduced from the experimental setup. Since we must assume the Yukawa potential to be only a minor correction to the Coulomb potential for small momentum transfer, we expect ℓ to be a macroscopic quantity. A bremsstrahlung experiment will never be the scattering of an electron at a *single* nucleus, but will always take place in a space with few nuclei. The *mean free path* length of a particle in a medium vacuum is a physically well-motivated choice for ℓ, in which case we typically have $\ell \approx 0.1$ m or, in natural units, $\ell = 5 \times 10^{11}$ MeV^{-1}, although there is no *a priori* fixation for particular geometries. At first glance, it is rather counterintuitive that a macroscopic quantity as ℓ can effect quantum mechanical experiments. It might be of interest that similar incidents are known in collision and particle physics (for reference, see footnote 29 in Chap. 3, p. 91 or Chap. 6.3, p. 259 of Ref. [42]).

B. Linear polarization

So far, we have just considered the case of a circularly polarized laser field. The case of linear polarization is discussed in [26]. Hence, we will rather shortly point out the main differences in comparison to circular polarization.

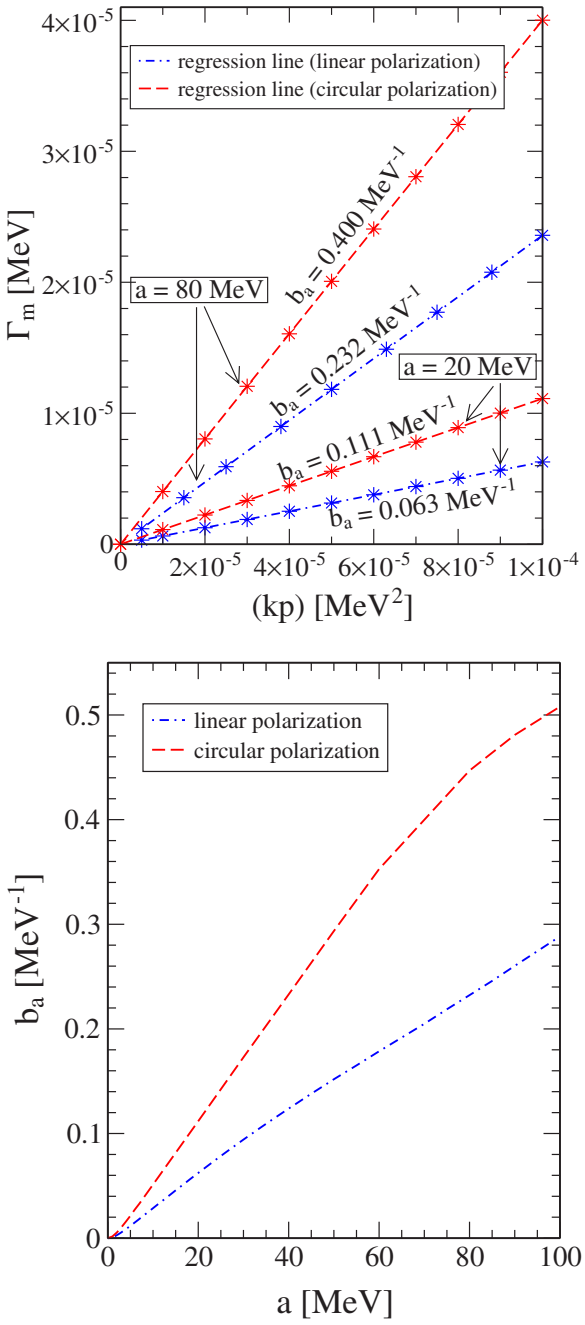

FIG. 3. (Color online) The imaginary mass shift Γ_m is a linear function of $k \cdot p$ as is clear from the upper diagram. The calculated values are marked with a star. Hence, it can be approximated by a linear function $\Gamma_m = b_a(k \cdot p)$ and can easily be implemented in the numerical evaluation of the cross section. The dependence of the slope b_a on the laser intensity a is shown in the lower diagram.

We obtain linear polarization for $\delta = 0$ in the laser four-vector potential Eq. (1),

$$A^\mu = a\epsilon_1^\mu \cos\phi. \tag{31}$$

The effective momentum q which naturally arises when calculating the Volkov solutions now reads

$$q = p + \frac{e^2 a^2}{4k \cdot p} k. \tag{32}$$

The expansion of the Volkov solutions leads to a different kind of generalized Bessel functions. They are defined by

$$A_s^0(\alpha,\beta) = \sum_{k=-\infty}^{\infty} J_{2k+s}(\alpha) J_k(\beta),$$

$$A_s^N(\alpha,\beta) = \tfrac{1}{2}[A_{s-1}^{N-1}(\alpha,\beta) + A_{s+1}^{N-1}(\alpha,\beta)]. \tag{33}$$

The difference between A^0 in the linear and B^0 in the circular case seems to be small. However, it turns out that A^0 cannot be reduced to a normal Bessel function as B^0 [43]. Thus, the numerical evaluation in the linear case is more demanding than in the circular one since we must evaluate one more infinite sum, namely the sum over k in the definition of A^0.

The final formula describing bremsstrahlung in a linear laser field looks very similar to the one for circular polarization. The (4×4)-matrix M in Eq. (19) describing the interaction with the nucleus and the emission of the bremsstrahlung photon, respectively, is modified in the following way:

$$M_t^{j,q}(X,\xi,\eta) = XA_t^0(\xi,\eta) + \frac{e^2 a^2}{4(k\cdot p_j)(k\cdot q)} \hat{k}X\hat{k}A_t^2(\xi,\eta) + \left(\frac{ea}{2k\cdot q} X\hat{k}\hat{\epsilon}_1 + \frac{ea}{2k\cdot p_j}\hat{\epsilon}_1\hat{k}X\right)A_t^1(\xi,\eta). \tag{34}$$

The steps leading to this result are the same as in the circular case. The calculations in the circular case are lengthier because more terms are involved; however, we would like to reemphasize that the numerical evaluation with linear polarization is more demanding.

We also note that the on-shell conditions in Eq. (24) and Eq. (25) for the intermediate electron do not depend on the polarization of the laser. However, since the definitions of the effective four momenta are different for the two polarizations according to Eq. (6) and Eq. (32), resonances do not occur at the same frequencies in general. Only for the special case of $\boldsymbol{k}_b \| \boldsymbol{k}$, the resonances for both cases will coincide because then the dependence of Eq. (24) and Eq. (25) on the effective momenta vanish (because of $q_{f,i}\cdot k_b = p_{f,i}\cdot k_b$).

Mass and energy regularization are implemented in the same way as described for circular polarization.

III. NUMERICAL RESULTS

We present some examples of the total cross section (23), considering the same parameters as in [26], namely a neodymium laser with a frequency of $\omega = 1.17$ eV, an energy of the initial electron of 10.0 times its rest mass m outside the laser field and a single proton $(Z=1)$ as a nucleus. As mentioned above, we employ $\boldsymbol{q}_i/|\boldsymbol{q}_i| = -\boldsymbol{k}/\omega$. In all of the following figures, the solid line refers to the laser-free (i.e., Bethe-Heitler) cross section, and cross sections in a circular laser field are denoted by a dashed line, whereas dotted-dashed lines denote linear polarization. The x axis of the spectra is the bremsstrahlung photon frequency ω_b scaled by the laser frequency ω. The stars appearing in the graphs indicate the calculated values at these points; especially, they indicate the finite value of the cross section exactly at the resonances in the spectra in Fig. 4 and Fig. 5. In Sec. III B, we set the amplitude a of the laser four-vector potential to 30 MeV. This corresponds to a laser intensity $I=(a\omega)^2$ of 7.58×10^{20} W/cm^2 in SI units [44] or, expressed in a frequently used, dimensionless parameter, $|e|a/m = 17.79$.

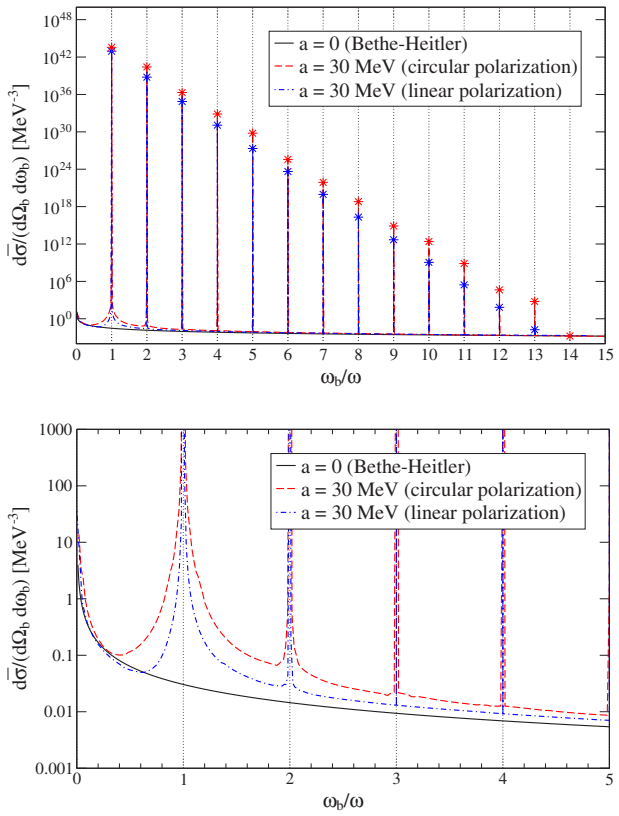

FIG. 4. (Color online) The total cross section for an emission angle $\theta_b = 179°$ of the bremsstrahlung photon. The lower diagram is a close-up of the upper diagram. Linear and circular polarization of the laser yield basically the same results. The background radiation in the laser-assisted cases is larger as the laser-free cross section. The screened Coulomb potential leads to finite values at the resonances. These are marked by stars.

A. Implementation of the imaginary mass shift

In order to regularize the electron propagators, we must calculate the imaginary mass shift Γ_m (26). The upper graph of Fig. 3 verifies our prior assertion: Γ_m is indeed a linear function of $(k\cdot p)$ in our range of interest, $(k\cdot p) < O(10^{-4}\ \text{MeV}^2)$. Hence, it can be rewritten as $\Gamma_m = b_a(k\cdot p)$ with b_a being the slope of the regression line.

The upper graph of Fig. 3 can only be used for a fixed laser intensity. If we are interested in the change of Γ_m with varying laser amplitude a, we get the lower graph. Here, we plotted the slope b_a of the regression line versus the laser intensity a because the slope does not depend on $(k\cdot p)$. Our

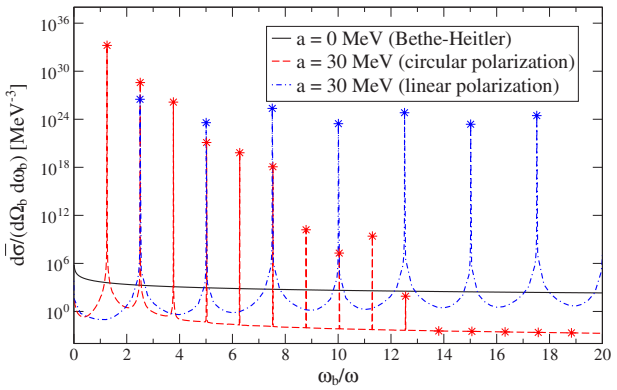

FIG. 5. (Color online) In this diagram, the bremsstrahlung photon is emitted with an angle $\theta_b=1°$, i.e. bremsstrahlung photon and laser photons are almost antiparallel. The resonances in the linear case survive much longer than in the circular case. The background radiation in both cases is several orders of magnitude smaller than in the laser-free case. This is in contrast to Fig. 4 where we consider an emission angle $\theta_b=179°$ of the bremsstrahlung photon.

results agree with the low-intensity calculations reported in Refs. [32,40].

For the implementation of Γ_m into the propagators, it is useful to find a function describing the curve b_a in Fig. 3 approximately. We find that the empirical ansatz $b_a=c_1\sqrt{a}+c_2a+c_3a^3$ with the three parameters c_1, c_2, and c_3 is rather suitable and we find

	c_1 (MeV$^{-3/2}$)	c_2 (MeV^{-2})	c_3 (MeV^{-4})
Linear	-1.12×10^{-3}	3.29×10^{-3}	-3.48×10^{-8}
Circular	-6.83×10^{-3}	7.23×10^{-3}	-1.44×10^{-7}

B. Total cross sections

We first discuss the spectrum for an emission angle $\theta_b=179°$ of the bremsstrahlung photon. From our formal considerations, we expect the emission of harmonics for this scattering geometry. This can clearly be seen in Fig. 4. We note that the spectra for linear and circular polarization are not only qualitatively but also quantitatively very similar, especially for increasing ω_b. This is due to the fact that the dependence on the laser polarization vectors $\boldsymbol{\epsilon}_1$ and $\boldsymbol{\epsilon}_2$ vanishes for the Compton part $M(\hat{\boldsymbol{\epsilon}}_b,\xi,\eta)$ [Eq. (19)] for this specific scattering geometry [45]. The resonances disappear after 13 peaks and the laser-assisted cross sections almost coincide with the laser free, namely Bethe-Heitler cross section. From a mathematical point of view, (generalized) Bessel functions suppress the peaks because their indices become considerably larger than their arguments with increasing ω_b as explained in Appendix A.

The next spectrum in Fig. 5 is basically the same as the one before, with the only difference that the bremsstrahlung photon is emitted nearly antiparallel to the laser photons, $\theta_b=1°$. Resonances for linear and circular polarization do not appear at the same frequency ω_b; their position can easily be calculated with Eq. (24) and Eq. (25). Two main differences compared to the previous spectrum attract attention. First, the resonances for circular polarization disappear rather quickly, whereas they survive much longer in the linear case. And second, the background radiation for both polarizations is several magnitudes smaller than in the laser-free case. The main contributions to the cross section (22) at a resonance come from the summands with $|\boldsymbol{q}_n|$ equal or close to zero as is clear from the previously described considerations. This means that there is effectively no momentum transfer onto the nucleus; hence, there is no Coulomb scattering. The matrix element S_{fi} reduces to a matrix element describing photon emission by an electron in a laser field. This explains the height and the structure of the resonances, in particular the exponential decay of the resonances seen in Fig. 4, as shown in [26].

In Fig. 5, the cross section for linear polarization shows many resonances which indicates that the whole process can be understood mainly in terms of laser-assisted Compton scattering. This is in sharp contrast to the circular case, where the background radiation generated by Coulomb scattering takes over after just two resonances and the resonances die away quickly.

C. Peculiar phenomena of the differential cross section

We now investigate the fully differential cross section given in Eq. (22). We fix the frequency ω_b according to the two cases of (i) a bremsstrahlung photon being exactly on the first resonance according to Eq. (25) and (ii) being exactly in the middle between the first and second resonance. As we consider the differential cross section, the direction of the outgoing electron also must be determined. Our conventions imply that $\theta_f=0°$ corresponds to forward scattering of the electron and $\theta_f=180°$ corresponds to backward scattering. The results of the calculations ($\theta_b=179°$) can be seen in Fig. 6.

The striking feature is in all cases the step at $a=33.7$ MeV for circular and at $a=47.7$ MeV for linear laser polarization. At this point, the differential cross section with $\theta_f=0°$ fall off to very low values (not shown in the graphs), whereas the ones with $\theta_f=180°$ increase suddenly from very low to quite significant values. In other words, we basically get forward scattering of the electron up to $a=33.7$ MeV or $a=47.7$ MeV, respectively, afterwards the electron is mostly scattered backwards.

The explanation of this unexpected behavior is in fact quite easy and intuitive. Going back to the definition of the effective momentum and considering only the x component (the direction of the x axis was defined according to the direction of the incident electron), we obtain

$$q_i^x = p_i^x - \frac{e^2a^2}{2k\cdot p_i}\omega. \tag{35}$$

For small a, q_i^x is a positive number; however, with increasing a, q_i^x becomes smaller and finally changes sign. The intuitive explanation of that effect is that the electron stops or travels backwards relative to the laser field for certain a. If it stops, the electron cannot be detected and the cross section goes to zero. The laser intensity a_0 at which this happens can be calculated as

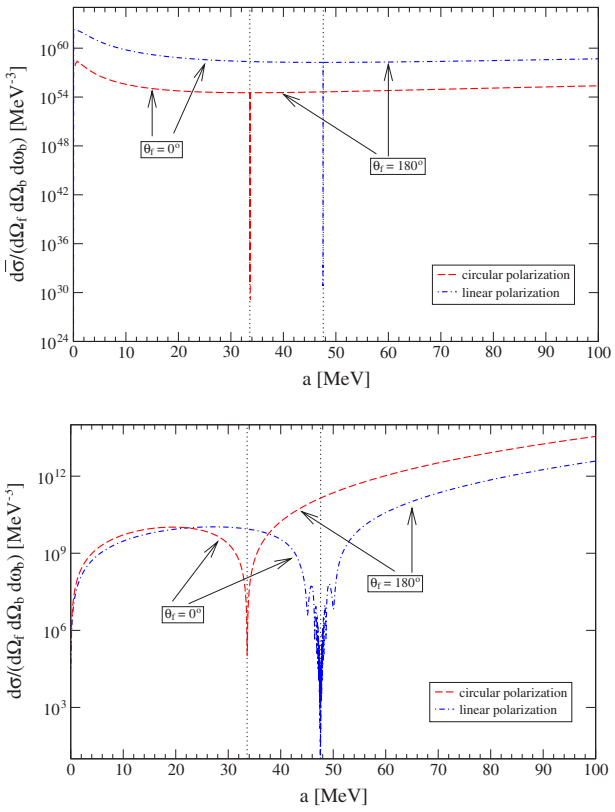

FIG. 6. (Color online) These graphs show the dependence of the differential cross section on the laser amplitude a. Therefore the frequency of the bremsstrahlung photon is fixed to be exactly on the first resonance according to Eq. (25) in the upper graph and to be exactly in the middle between the first and second resonance in the lower graph. In all cases, the bremsstrahlung photon is emitted with an angle $\theta_b = 179°$. The dip (dotted lines) in the cross sections at $a = 33.7$ MeV for circular and at $a = 47.7$ MeV for linear polarization is due to zero effective momentum of the electron in the laser field.

$$0 \overset{!}{=} p_i^x - \frac{e^2 a_0^2}{2k\cdot p_i}\omega \Leftrightarrow a_0 = \sqrt{\frac{2p_i^x(k\cdot p_i)}{e^2\omega}}$$
$$= \sqrt{\frac{2\sqrt{E_i^2 - m^2}(E_i + \sqrt{E_i^2 - m^2})}{e^2}}$$
$$\approx \frac{2\gamma m}{e} \quad \text{for electrons with } E_i = \gamma m \gg m. \tag{36}$$

The corresponding calculation for linear polarization yields an additional factor $\sqrt{2}$: $a_0 = 2\sqrt{2}\gamma m/e$. In our case, $\gamma = 10.0$ which yields $a_0 = 33.7$ MeV for circular and $a_0 = 47.7$ MeV for linear polarization.

We note that the total, i.e., the integrated cross section over d^3q_f will cover up the jump at a_0; only at off-resonance frequencies ω_b, some traces of the jump might be detectable as the lower graph of Fig. 6 indicates. In the evaluation of the total cross section, we use the equality $d^3q_f = d^3p_f$. However, in the differential cross section, we must specify the angles for the effective four momentum q_f. In order to compare our results with an experiment, we must convert q_f to a real four momentum p_f, which amounts to solving Eq. (6) for p_f. Owing to $k\cdot q_f = k\cdot p_f$, this is easy, $p_f = q_f - e^2a^2/(2k\cdot q_f)k$ for circular polarization and $p_f = q_f - e^2a^2/(4k\cdot q_f)k$ for linear polarization.

IV. CONCLUSIONS

Our goal in this paper was the evaluation of laser-assisted bremsstrahlung for—in principle—arbitrary laser amplitude a. In that case, as shown in Appendix B, we do not expect any recollision effects of the electron and the nucleus. Hence, a semiclassical model such as the three-step model cannot be applied for the analysis of this process. Rather, we must apply the S-matrix formalism of QED. The solutions of the Dirac equation in an external field lead to the initial and final states, the so-called Volkov states Eq. (4), and an intricate Dirac-Volkov propagator Eq. (11). In order to make a numerical evaluation feasible, we must expand the Volkov solutions in plane waves. This leads us to the generalized Bessel functions in Eqs. (8) and (33) and slowly convergent sums.

In order to obtain finite values at the resonances, two conceptual challenges must be addressed. (i) We regularize the electron propagator by introducing an imaginary mass and energy shift according to Eqs. (26) and (27). (ii) Furthermore, the Coulomb photon also had to be regularized, and this was done by employing a screened Coulomb potential, as given in Eq. (14). As an outlook, it would be interesting to compare the results here with calculations employing a finite laser pulse and an energy spread of the initial electron energy, since this would provide a natural cutoff for the resonances. This would require a slightly different approach, similar to the treatment of laser-induced Compton scattering performed in [41].

We calculate the total probability W_γ of photon emission by an electron in a laser field up to laser amplitudes $a = 100$ MeV, see Fig. 3. This corresponds to intensities of 8.54×10^{21} W/cm^2 with our choice of $\omega = 1.17$ eV. This process has only been evaluated for rather small laser intensities so far [32,40]. Our results, including the various regularizations, also constitute a necessary step toward any higher-order processes involving electron propagators in an external plane wave field.

The spectra Fig. 4 and Fig. 5 for the emission angles $\theta_b = 179°$ and 1° of the bremsstrahlung photon show the general structure we expect from theoretical considerations. It can easily be shown that we always get harmonics in the *rest frame* of the electron in a very good approximation. In the laboratory frame however, a significant number of harmonics only appears for parallel propagation of the bremsstrahlung photon and laser photons according to Eqs. (24) and (25). This condition is fulfilled for $\theta_b = 179°$ (see Fig. 2). From the point of view of the initial electron, the bremsstrahlung photon is backscattered then; it is forward scattered relative to the laser photons. For this particular scattering geometry, circular and linear laser polarization yield almost the same spectrum because the dependence on the laser polarization vectors vanish for the Compton part.

In general, the Doppler effect implies that the greater the angle θ_b is, the smaller is the spacing between the resonances. The contributions to the cross section with zero-momentum transfer onto the nucleus $|\boldsymbol{q}_n|=0$ determine the height and structure of the resonances. Hence, Coulomb scattering can be neglected for a qualitative understanding at these particular points and the basic process taking place is laser-assisted Compton scattering [8,26].

To conclude, let us remark that a closer look at a curious feature of the fully differential cross section reveals that if we fix all parameters and only vary the laser amplitude a, we observe a sharp step in the cross section at $a=33.7$ MeV for circular and at $a=44.7$ MeV for linear polarization, respectively. In an intuitive picture, this step corresponds to exactly that intensity at which the electron is classically at rest relative to the laser field.

ACKNOWLEDGMENT

The authors thank Professor A. I. Milstein for helpful discussions. One of the authors (U. D. J.) acknowledges support from the Deutsche Forschungsgemeinschaft (Heisenberg program).

APPENDIX A: GENERALIZED BESSEL FUNCTIONS

A definition of Bessel functions of the first kind is

$$J_n(x)=\left(\frac{x}{2}\right)^n\sum_{j=0}^{\infty}\frac{(-1)^j}{j!\Gamma(j+n+1)}\left(\frac{x}{2}\right)^{2j}. \tag{A1}$$

We consider only Bessel functions with integer index so that we can write $\Gamma(j+n+1)=(j+n)!$. They possess the Jacobi-Anger expansion

$$\exp(iz\cos\phi)=\sum_{s=-\infty}^{+\infty}i^sJ_s(z)\exp(is\phi),$$

$$\exp(iz\sin\phi)=\sum_{s=-\infty}^{+\infty}J_s(z)\exp(is\phi). \tag{A2}$$

Hence, we can easily expand

$$\exp(i\xi\sin\phi+i\eta\cos\phi)=\sum_{s=-\infty}^{+\infty}B_s^0(\xi,\eta)\exp(is\phi),$$

$$\cos\phi\exp(i\xi\sin\phi+i\eta\cos\phi)=\sum_{s=-\infty}^{+\infty}B_s^1(\xi,\eta)\exp(is\phi),$$

$$\sin\phi\exp(i\xi\sin\phi+i\eta\cos\phi)=\sum_{s=-\infty}^{+\infty}B_s^2(\xi,\eta)\exp(is\phi), \tag{A3}$$

with the three generalized Bessel functions $B_s^0(\xi,\eta)$, $B_s^1(\xi,\eta)$, and $B_s^2(\xi,\eta)$ which are defined in Eq. (8). In this particular case, the infinite sum over the product of the two Bessel functions in the definition of B_s^0 can be reduced to a single Bessel function with the help of Graf's addition theorem [46],

$$J_s(z)\left(\frac{x-ye^{-i\phi}}{x-ye^{i\phi}}\right)^{(1/2)s}=\sum_{n=-\infty}^{+\infty}J_{s+n}(x)J_n(y)e^{in\phi} \tag{A4}$$

with $z=(x^2+y^2-2xy\cos\phi)^{1/2}$ and $|ye^{\pm i\phi}|<|x|$. If we apply this to B_s^0, we obtain $B_s^0(\xi,\eta)=J_{-s}(\sqrt{\xi^2+\eta^2})(\frac{-\xi-\eta i}{-\xi+\eta i})^{(1/2)s}$. Using well-known properties of Bessel functions, it is easy to prove that $B_s^{0*}(\xi,\eta)=B_s^0(\xi,-\eta)$ and $B_{-s}^0(\xi,\eta)=B_s^0(-\xi,\eta)$. Similar relations also hold for B_s^1 and B_s^2.

Sum rules can be found for generalized Bessel functions by repeated use of Graf's addition theorem. Here, we will just consider the special case that occurs if one argument of one of the generalized Bessel functions is zero. This is sufficient in our case because of our choice of the polarization vectors and $\eta_f=0$. Then, we obtain

$$\sum_{n=-\infty}^{+\infty}B_{n+s}^0(\alpha,\beta)B_{n+t}^0(\gamma,\delta)\overset{\delta=0}{=}B_{s-t}^0(\alpha-\gamma,\beta). \tag{A5}$$

Similar expressions can be found for every infinite sum over any product of the three generalized Bessel functions.

An asymptotic expansion of Bessel functions of large order $(n\to\infty)$ and fixed argument x is [47]

$$J_n(x)\sim\frac{1}{\sqrt{2\pi n}}\left(\frac{ex}{2n}\right)^n. \tag{A6}$$

From this relation, we can conclude that Bessel functions decrease very rapidly if $|n|>|x|$. In our numerical evaluation, we use this property to find summation limits up to which we must sum and then truncate the infinite sum. Only because of this behavior, it is possible to numerically calculate the laser-dressed bremsstrahlung cross section.

APPENDIX B: CLASSICAL TRAJECTORY OF A CHARGED PARTICLE IN A LASER FIELD

We start from the relativistic equation of motion for a charged particle in a laser field,

$$m\frac{du^\mu(\tau)}{d\tau}=-eF^\mu{}_\nu u^\nu(\tau). \tag{B1}$$

u is the four velocity, τ is the proper time, and $F^{\mu\nu}=\partial^\mu A^\nu-\partial^\nu A^\mu$ is the field-strength tensor with $A^\mu(\phi)=a(\delta\epsilon_1^\mu\cos\phi+\epsilon_2^\mu\sin\phi)$. We solve this differential equation for an arbitrary polarization δ in the same way as in [48] for linear polarization. The resulting trajectory depends on the initial four velocity $u^\mu(0)$ and the laser phase ϕ,

$$x^{\mu}(\phi) = \frac{u^{\mu}(0)}{k\cdot u(0)}\phi + \frac{ea}{m}\delta(\sin\phi-\phi)\frac{\epsilon_1^{\mu}}{k\cdot u(0)} - \frac{ea}{m}(\cos\phi-1)\times\frac{\epsilon_2^{\mu}}{k\cdot u(0)} - \frac{ea}{m}\Bigg(\delta\epsilon_1\cdot u(0)(\sin\phi-\phi) - \epsilon_2\cdot u(0)\times(\cos\phi-1) - \frac{ea}{8m}[(\delta-1)\sin(2\phi) - 8\delta\sin\phi + (6\delta+2)\phi]\Bigg)\frac{k^{\mu}}{[k\cdot u(0)]^2}. \quad \text{(B2)}$$

Since we consider relativistic intensities, the drift velocity induced by the $\vec{B}$ field must not be neglected. An electron which is initially at rest travels approximately 1.6×10^{6} MeV^{-1} during one laser cycle due to the drift velocity. If we compare this with the *first Bohr radius* $a_0=1/(Z\alpha m_e)\approx 270$ MeV^{-1} ($Z=1, a=30$ MeV), we see that this distance is roughly 6000 times greater than the Bohr radius. Hence, to a very good approximation, there is only one interaction between electron and nucleus possible. Recollision processes can be neglected.

[1] P. Agostini, F. Fabre, G. Mainfray, G. Petite, and N. K. Rahman, Phys. Rev. Lett. **42**, 1127 (1979).

[2] D. B. Milosevic, G. G. Paulus, D. Bauer, and W. Becker, J. Phys. B **39**, 203 (2006).

[3] B. W. Shore and P. L. Knight, J. Phys. B **20**, 413 (1987).

[4] A. McPherson, G. Gibson, H. Jara, U. Johann, T. S. Luk, I. A. McIntyre, K. Boyer, and C. K. Rhodes, J. Opt. Soc. Am. B **4**, 595 (1987).

[5] Y. I. Salamin, S. X. Hu, K. Z. Hatsagortsyan, and C. H. Keitel, Phys. Rep. **427**, 41 (2006).

[6] L. S. Brown and T. W. B. Kibble, Phys. Rev. **133**, A705 (1964).

[7] P. Panek, J. Z. Kamiński, and F. Ehlotzky, Phys. Rev. A **65**, 022712 (2002).

[8] A. I. Nikishov and V. I. Ritus, Zh. Eksp. Teor. Fiz. **46**, 776 (1963) [Sov. Phys. JETP **19**, 529 (1964)].

[9] C. Szymanowski, V. Véniard, R. Taïeb, A. Maquet, and C. H. Keitel, Phys. Rev. A **56**, 3846 (1997).

[10] P. Panek, J. Z. Kamiński, and F. Ehlotzky, Phys. Rev. A **65**, 033408 (2002).

[11] V. P. Oleĭnik, Zh. Eksp. Teor. Fiz. **52**, 1049 (1967) [Sov. Phys. JETP **25**, 697 (1967)].

[12] J. Bös, W. Brock, H. Mitter, and T. Schott, J. Phys. A **12**, 715 (1979).

[13] P. Panek, J. Z. Kamiński, and F. Ehlotzky, Phys. Rev. A **69**, 013404 (2004).

[14] V. N. Baĭer, V. M. Katkov, and V. M. Strakhovenko, Yad. Fiz. **14**, 1020 (1971), [Sov. J. Nucl. Phys. **14**, 572 (1972)].

[15] V. I. Ritus, Nucl. Phys. B **44**, 236 (1972).

[16] V. M. Katkov and V. M. Strakhovenko, Yad. Fiz. **25**, 1245 (1977) [Sov. J. Nucl. Phys. **25**, 660 (1977)].

[17] H. Terashima, Phys. Rev. D **60**, 084001 (1999).

[18] M. Kalinski, Laser Phys. **15**, 1367 (2005).

[19] R. Schützhold, G. Schaller, and D. Habs, Phys. Rev. Lett. **97**, 121302 (2006).

[20] R. V. Karapetyan and M. V. Fedorov, Zh. Eksp. Teor. Fiz. **75**, 816 (1978) [Sov. Phys. JETP **48**, 412 (1978)].

[21] I. Bialynicki-Birula, M. Kaliński, and J. H. Eberly, Phys. Rev. Lett. **73**, 1777 (1994).

[22] Z. Bialynicka-Birula and I. Bialynicki-Birula, Phys. Rev. A **56**, 3623 (1997).

[23] S. P. Roshchupkin, Yad. Fiz. **41**, 1244 (1985) [Sov. J. Nucl. Phys. **41**, 796 (1985)].

[24] S. P. Roshchupkin and O. B. Lysenko, Zh. Eksp. Teor. Fiz. **116**, 1210 (1999) [J. Exp. Theor. Phys. **89**, 647 (1999)].

[25] S. P. Roshchupkin, Laser Phys. **12**, 498 (2001).

[26] E. Lötstedt, U. D. Jentschura, and C. H. Keitel, Phys. Rev. Lett. **98**, 043002 (2007).

[27] E. S. Sarachik and G. T. Schappert, Phys. Rev. D **1**, 2738 (1970).

[28] D. M. Volkov, Z. Phys. **94**, 250 (1935).

[29] W. B. Berestetski, E. M. Lifschitz, and L. P. Pitajewski, *Quantenelektrodynamik (Band IV der Lehrbuchreihe über Theoretische Physik von L. D. Landau und E. M. Lifschitz)*, 5th ed. (Akademie-Verlag, Berlin, 1986).

[30] V. I. Ritus, Ann. Phys. (N.Y.) **69**, 555 (1972).

[31] H. Mitter, Acta Phys. Austriaca, Suppl. **14**, 397 (1975).

[32] W. Becker and H. Mitter, J. Phys. A **9**, 2171 (1976).

[33] H. A. Bethe and W. Heitler, Proc. R. Soc. London, Ser. A **146**, 83 (1934).

[34] P. B. Corkum, Phys. Rev. Lett. **71**, 1994 (1993).

[35] We neglect the indices i,f to distinguish between initial and final electron. However, one should keep in mind that all energies and momenta are labelled with i or f.

[36] H. R. Reiss and J. H. Eberly, Phys. Rev. **151**, 1058 (1966).

[37] Since the Bethe-Heitler cross section is derived using a Coulomb potential, the laser-assisted bremsstrahlung cross section coincides with the Bethe-Heitler cross section in the limit $\ell\to\infty$ and a vanishing laser field. Note that the Yukawa potential modifies the Bethe-Heitler cross section only close to the infrared divergences, i.e., if the momentum transfer $\boldsymbol{q}$ is close to zero.

[38] This follows from the relation $\mathrm{Tr}[\hat{a}_1\hat{a}_2\cdots\hat{a}_n] = (a_1\cdot a_2)\mathrm{Tr}[\hat{a}_3\cdots\hat{a}_n] - (a_1\cdot a_3)\mathrm{Tr}[\hat{a}_2\hat{a}_4\ldots\hat{a}_n] + \cdots + (a_1\cdot a_n)\mathrm{Tr}[\hat{a}_2\cdots\hat{a}_{n-1}]$ and is true for any general four-vector a_n. In cases like $a_n=(1,0,0,0)$ or when some natural cancellations occur after the traces have been taken, it is advantageous to perform the Dirac algebra symbolically even if a large number of matrices are involved. However, the cancellations are not observed in the current investigation.

[39] In fact, it can be shown easily that we always have harmonic generation independent of $\tilde{n}_b$ in the rest frame of the electron if we neglect the $k\cdot\tilde{n}_b$ term in the denominator. This is well justified as long as the number of resonances is not too high because $Q_{i,f}\sim O(1\text{ MeV}) - O(10\text{ MeV})$ whereas $\omega_b \sim O(10^{-6}\text{ MeV}) - O(10^{-3}\text{ MeV})$ for $n+s, s\lesssim 10^4$.

[40] V. A. Lyul'ka, Zh. Eksp. Teor. Fiz. **67**, 1638 (1974) [Sov. Phys. JETP **40**, 815 (1975)].
[41] N. B. Narozhnyĭ and M. S. Fofanov, Zh. Eksp. Teor. Fiz. **110**, 26 (1996) [J. Exp. Theor. Phys. **83**, 14 (1996)].
[42] M. L. Goldberger and K. M. Watson, *Collision Theory*, 1st ed. (Wiley, New York, 1964).
[43] This is due to the factor 2 in the index of Eq. (31) so that Graf's addition theorem cannot be applied [see Eq. (A4)].
[44] To be precise, this is only true for circular polarization. In the linear case, one must calculate the average over one laser cycle which yields one-half of that value.
[45] If $\theta_b \approx 180°$, then not only $\boldsymbol{\epsilon}_{1,2} \perp \boldsymbol{k}$ but also $\boldsymbol{\epsilon}_{b,(1,2)} \perp \boldsymbol{k}$.
[46] H. Bateman, *Higher Transcendental Functions, Volume II* (McGraw-Hill, New York, 1953).
[47] M. Abramowitz and I. A. Stegun, *Handbook of Mathematical Functions* (Dover, New York, 1972).
[48] C. Itzykson and J.-B. Zuber, *Quantum Field Theory*, 2nd ed. (Dover, New York, 2006).